Soils and Foundations 2016;56(4):627–639

HOSTED BY

ELSEVIER

CrossMark

The Japanese Geotechnical Society

Soils and Foundations

www.sciencedirect.com
journal homepage: www.elsevier.com/locate/sandf

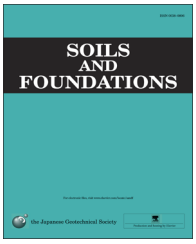

Technical Paper

Track-bed mechanical behaviour under the impact of train at different speeds

Francisco Lamas-Lopez[a,b,*], Yu-Jun Cui[a], Nicolas Calon[b], Sofia Costa D'Aguiar[c], Matheus Peixoto De Oliveira[c], Tongwei Zhang[a]

[a]*Ecole des Ponts ParisTech, Laboratoire Navier/CERMES, Marne-la-Vallée, France*
[b]*SNCF – Engineering, Département Ligne, Voie et Environnement, La Plaine St. Denis, France*
[c]*SNCF – Research & Development, Division Auscultation, Modélisation & Mesures, Paris, France*

Received 16 September 2015; received in revised form 3 March 2016; accepted 17 March 2016
Available online 24 August 2016

Abstract

This paper aims to study the influence of train speed on the mechanical behaviour of track-bed materials based on field data recorded at a representative site of the conventional French network. Capacitive accelerometers and soil pressure gauges were installed in track-bed layers. The Intercity train was selected to perform this study as it is the most frequent train running on this site. In total, 1790 records corresponding to Intercity train passages were taken into account, with train speeds ranging from 60 to 200 km/h. The vertical strains of different layers were estimated by integrating the signals of accelerometers installed at different depths. It is observed that when train speed increased in the considered range, the traffic loadings, in terms of dynamic stress transmitted to track-bed materials, were amplified about 10%. However, the vertical strains of track-bed materials were also amplified by 2 in the same range of speeds. These amplifications appear mainly in shallower layers. The stress–strain amplitude ratios for all the recorded trains were calculated to analyse the evolution of resilient moduli (M_r) of track-bed materials. It is found that M_r of interlayer soil decreased by approximately 25% when train speed increased from 60 to 200 km/h.

Keywords: Conventional lines; Track-bed materials; Train speed; Mechanical behaviour; *'In-situ'* experimentation; Resilient modulus

1. Introduction

The European railway networks mostly involve conventional lines, with a service speed limited to 220 km/h (only 7000 km over almost 200.000 km of European lines are High-Speed lines, with higher service speeds). For instance, in France, almost 94% (about 29.800 km) of the operational lines are conventional ones (Duong et al., 2014a, 2014b). Seeking to reduce the travel time in railway transportation, the European railway administrators look to increase the speed of the trains. Several studies of train speed upgrade on European conventional lines have been conducted in the past (Hall and Bodare, 2000; Hendry et al., 2010; Madshus and Kaynia, 2000). However, the speed upgrade impact on the mechanical behaviour of track-bed materials (loading and response amplifications with train speed) is still an open question.

In order to better understand the mechanical behaviour of the materials composing the track-bed in the context of optimization of maintenance operations, the French railway company (SNCF) launched the 'INVICSA' project in 2011, aiming to investigate the train speed impact on the behaviour

*Corresponding author at: Ecole des Ponts ParisTech, Laboratoire Navier/CERMES, Marne-la-Vallée, France.
E-mail addresses: lamas1987@gmail.com (F. Lamas-Lopez), cui@cermes.enpc.fr (Y.-J. Cui), nicolas.calon@sncf.fr (N. Calon), sofia.costadaguiar@sncf.fr (S. Costa D'Aguiar), matheus.pxto@gmail.com (M. Peixoto De Oliveira), zhangt@cermes.enpc.fr (T. Zhang).
Peer review under responsibility of The Japanese Geotechnical Society.

http://dx.doi.org/10.1016/j.sandf.2016.07.004

of conventional line tracks. Note that the main difference of track-bed between the conventional and new high speed lines is the existence of a heterogeneous "interlayer" below the ballast layer in the former (Cui et al., 2014). This layer was created over time between the ballast and the subgrade (Trinh et al., 2012), mainly by the interpenetration of ballast grains and fines from subgrade as well as from ballast attrition (Cui et al., 2013; Duong et al., 2014a, 2014b). The nature and thickness of the interlayer depends on the geological conditions and the loading history of track (Costa et al., 2015; Hall, 2003; Hendry et al., 2013; Madshus and Kaynia, 2000). Moreover, the interlayer and subgrade properties will determine the site surface wave velocity which is directly related to the critical speed at which the mechanical response of materials reaches a local maximum under train loading. The acceptance of speed upgrade is strongly conditioned by the mechanical properties of track-bed materials as their stiffness (Costa et al., 2015). Very often, the soil stiffness is determined through the shear wave velocity (Gunn et al., 2003; Kim et al., 2001; Sawangsuriya, 2012).

Several authors have studied the behaviour of track-bed materials with train passages (Bowness et al., 2007; Hendry, 2007; Le Pen, 2008; Le Pen et al., 2014; Powrie et al., 2007; Priest et al., 2010). Field tests tend to be adopted in the study of the mechanical behaviour of track-bed materials under train loading. Fröhling (1997) studied the effect of spatial variation of track stiffness on track degradation. Aw (2007) investigated the impact of subgrade soft soil saturation on the track behaviour in terms of mud-pumping. He showed that larger surface deflections occurred when the subgrade was composed of soft soils with low shear wave velocity or low stiffness. A photo-sensitive array method was applied after some stability problems due to the presence of soft soils in conventional tracks by Hendry (2011) and extensometers were used by Hendry et al. (2010, 2013). It was observed that the sleeper deflection increased with the increase of train speed, depending mainly on the subgrade mechanical properties, such as elastic modulus and damping ratio. Madshus and Kaynia (2000) showed the key role of surface wave velocity in the amplification of track deflection. When the surface wave velocity had the lowest value in the first meter of a track section, the track deflections reached their maximum values. The amplifications due to train speed and surface wave velocity were summarized by Connolly et al. (2014) and Madshus et al. (2004). The track typology was also recognized as an influencing factor for the deflection amplifications (Kempfert and Hu, 1999). Ballasted tracks transmit higher loads to the firsts track-bed layers compared to slab-tracks and consequently, and the response amplification of train loads could bring more significant defects if the speed upgrade is carried out for ballasted tracks.

Some semi-analytical models for track deflections were developed by Sheng et al. (2004) and Costa et al. (2015). Numerical analyses using FEM were also performed to investigate the influence of train speed on the behaviour of tracks (Alves Costa et al., 2010; Connolly et al., 2013; Kouroussis, 2009; Woodward et al., 2013). The results showed a decrease in the elastic shear moduli of track-bed materials with the increase intrain speed (Alves Costa et al., 2010).

Strain measurement using multi-depth deflectometers and strain gauges were carried out in several studies to analyse the contribution of each individual substructure layer to the differential settlement of the railway platform (Fröhling, 1997; Hall and Bodare, 2000; Mishra et al., 2014; Priest et al., 2010). Moreover, real scale physical models were developed to analyse the recorded load amplifications in the configuration of concrete slab (Bian et al., 2014; Chen et al., 2013; Xu et al., 2013).

Nevertheless, to the authors' knowledge, few analyses have been conducted on the evolution of mechanical behaviour of real tracks in terms of stress and strain amplitudes. The evolution of the recorded measurements over time, their dispersion and consistence need to be examined in-depth. Moreover, it is interesting to estimate such mechanical properties as the resilient modulus based on the records of sensors embedded in track-beds. In this study, firstly, the stress amplitude measurements under different axle types (locomotive and coach) were analysed. Then, the evolution of deflections with speed increase under both types of axle loads was calculated from the records of accelerometers installed at different depths. The vertical strain amplitudes of interlayer and subgrade soils were estimated from the calculated deflections at different levels of the track. The resilient modulus (M_r) based on the vertical stress and strain amplitudes was estimated for an Intercity train running over the experimental site during 5 months at a speed ranging from 60 to 200 km/h. Finally, the averages of kinematics variables (such as acceleration, particle velocity and deflection amplitude), the mechanical parameters (such as stress and strain amplitudes) and their influence on the resilient modulus and damping ratio are discussed in this paper.

2. Experimental site

The 'INVICSA' project involves setting up a full scale field experimental site on a conventional line track. The experimental site was chosen within the 30000 km French conventional network (Cui et al., 2014; Lamas-Lopez et al., 2014a, 2014b). The selection criteria were related to the speed limit on the site (200 km/h, close to the maximum speed for the conventional lines), the main characteristics of track (alignment, cutting zone, proximity to electrical connection) and the state of the rails and sleepers (without special maintenance operations since the last renewal works). The alignment of track is important to ensure that both rails of the track are loaded at the same level. The experimental site finally selected was located in Vierzon, France, at KP+187 of the line connecting Orléans and Montauban. The instrumented section is 30 m long. Dynamic sensors such as capacitive accelerometers and soil stress sensors were installed at three different depths along the experimental site. The capacitive accelerometers were selected rather than piezo-electric accelerometers in order to better register the low-frequency range, where most of the displacements due to long wavelengths are produced.

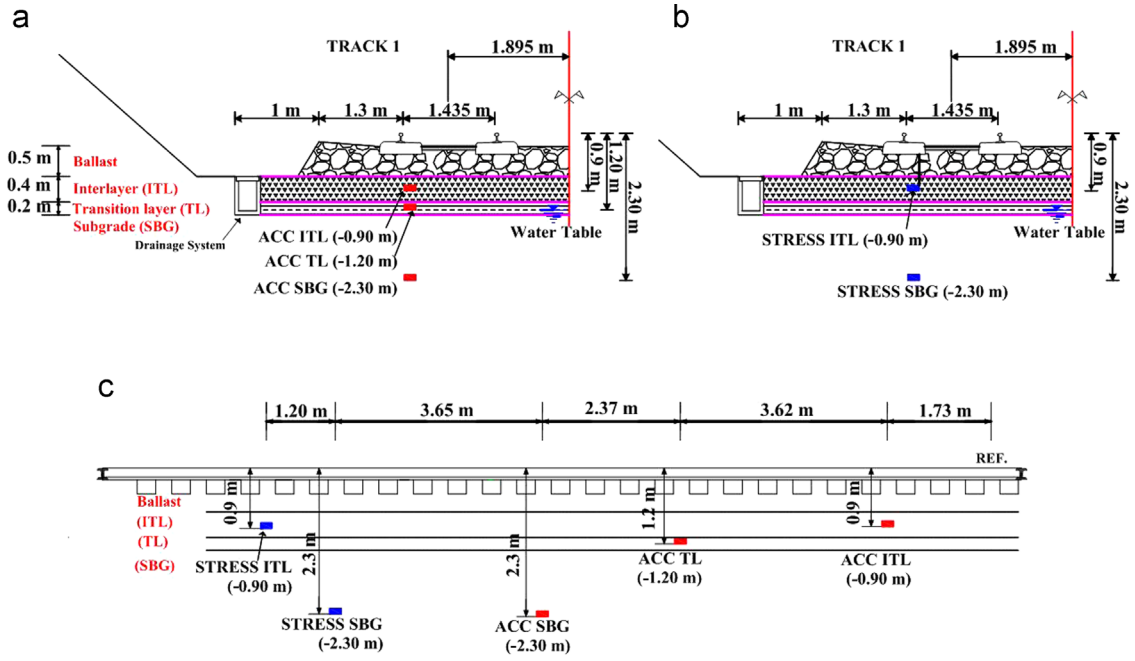

Fig. 1. (a) Cross section and (b) Longitudinal section of the experimentation zone with installation positions of the sensors used in this study. Reference point is spotted as 'REF.'

The soil pressure gauges were 100 *mm* in diameter (adapted to the maximum grain size in interlayer) and were oriented in vertical position. Moreover, these stress sensors were able to measure dynamic stresses up to 200 kPa, considerably larger than the expected stress amplitudes of about 20 kPa under train loading and to support the static load of the upper soil at that depth (about 10 kPa). In addition, in order to identify each axle from every registered signal (stress and acceleration), strain gauges werealso glued to the rails. Different kinds of embedded sensors were installed in different boreholes as described in Cui et al. (2014) and Lamas-Lopez et al. (2014). A representative cross section and a representative longitudinal section are presented in Fig. 1. The installation depths and distances between the sensors are also indicated in Fig. 1. All sensors were installed under the same track-side and received the same train loading. A previous site prospection (Lamas-Lopez et al., 2016) revealed that the track-bed is composed of about 500 *mm* ballast, 400 *mm* interlayer (ITL) and 200 *mm* transition layer (TL) that overlies the subgrade (SBG). The fresh ballast is composed of coarse grains with diameter ranging from 50 to 31.5 *mm*. The ITL is composed of ballast grains with a maximum diameter of 50 mm, mixed with silty sand from SBG and from ballast attrition. Thus, this ITL is the result of ballast attrition and the interpenetration of the subgrade fines over time (Duong et al., 2013; Trinh, 2011; Trinh et al., 2012). In ITL, approximately 10% of the particles are finer than 80 μm, and the D_{50} is around 10 *mm*. The dry density of ITL is very high, reaching $\rho_d = 2.4\ Mg/m^3$ (Trinh, 2011; Trinh et al., 2012). While the TL contains the same fines as ITL, it also includes a quantity of grains from ballast attrition (larger than 20 mm diameter) limited to 15%. The D_{50} is 1 mm for the TL. The SBG is constituted by a silty sand with a D_{50} of 0.3 *mm* and a plasticity index (PI) of 18. The water table in the area was stable during the test period, and located at a depth of 1.20 m. The bottom surface of the drainage system is also located at 1.20 *m*, indicating that the drainage system worked well. Therefore, the SBG is fully saturated. The confining pressure of the track-bed materials is assumed to be lower than 50 kPa for the first 2 *m* depth (Duong et al., 2013; Trinh et al., 2012). The dry density of SBG is much lower than ITL (Duong et al., 2014a, 2014b) because of the different depths (consequently, the arriving loads to each track-bed layer are lower in amplitude in the case of SBG) and also depends on soil constitution (SBG soils do not contain ballast grains).

Table 1
Technical specifications of installed accelerometers.

	Brand & model	Capacity	Dimensions
Stress sensors	TML KDD-PA	200 kPa	Diam.: 100 mm Height: 20.5 mm
Capacitive accelerometer	TML ARH-10A	± 1 g	16 × 16 × 28 mm^3

In this study, the measurements from two embedded soil stress sensors and three embedded capacitive accelerometers (Fig. 1) were analysed. The soil stress sensors were installed in ITL ($z = -0.90\ m$) and in SBG ($z = -2.3\ m$). The capacitive accelerometers were installed in ITL ($z = -0.90\ m$), in TL ($z = -1.20\ m$) and in SBG ($z = -2.3\ m$). The technical specifications of the capacitive accelerometers and soil stress sensors are shown in Table 1. The soil stress sensor is 100 *mm* in diameter, and was fitted to the biggest grains in ITL (about 50 *mm*). Fontainebleau sand of 1 mm diameter was used to fill the first 5 cm of borehole bottom prior to the installation of the sensor to ensure good contact with the soil.

The extracted soils from ITL and TL were replaced by a soil prepared in the laboratory. The filling soil in boreholes was compacted with a rod during the filling at the optimum moisture content (OPM). The procedure for material re-filling was identical for all boreholes in order to control the density, the grain size distribution and the fines plasticity. Since the size of boreholes (where sensors are embedded) is $\phi = 110\ mm$, a negligible size compared to the entire track, it is believed that the peak values of the sensors (under axle loading) are not significantly influenced by the presence of boreholes. The laboratory material was chosen to represent the *'in-situ'* soil on one hand, and to obtain a density by compaction close to the *'in-situ'* one ($\rho_d = 2\ Mg/m^3$) on the other hand. For this purpose, grains larger than 2 *mm* were removed. In addition, the grain size distribution and the plasticity index was kept the same as those of the *'in-situ'* soil. A waiting period of six months was observed prior to the first measurements in order to facilitate the homogenization with the surrounding soil after more than 300.000 axle's loadings. The ballast layer (first 500 mm), which strongly influences the behaviour of the rest of track-bed materials (Alves Fernandes, 2014), remained unchanged after sensor installation. More details about the installation method can be found in Cui et al. (2014) for a different site at Moulin Blanc. Capacitive accelerometers were used to reliably measure the frequencies in the low range from 1 to 10 *Hz*. This is important for the accuracy of displacement determination by the integration method. More information about the selection of sensors and site selection can be found in Lamas-Lopez et al. (2014).

In order to describe other mechanical properties of the experimental site, different geophysical tests were carried out. From the MASW tests (multichannel analysis of surface waves), it was found that the average shear wave velocity in the first 5 *m* depth was about 180 *m/s*, or more than 3 times greater than the maximum train speed on the site ($v_{max} = 200$ km/h). This value is close to the surface Rayleigh wave velocity or the critical speed on the site. Consequently, if a train could run on the site at that speed, the track mechanical response may reach a local maximum due to the resonance of the structure (Costa et al., 2015; Hendry, 2007). The response amplification at lower sub-Rayleigh speeds (related to the critical speed of a site) is discussed in the following sections.

3. Selected train

To analyse the loading amplitude evolution and track response under the impact of loadings from trains running at different speeds, the Intercity train was selected. This train is the most common type in the experimental site, since it represents more than 43% of the total train passages. The other trains running on the site are freight and maintenance trains (21%), regional trains Z7300 (20%), Z21500 (8%) and Z27500 (6%) and 'TGV-Réseau' trains (2%). The Intercity train consists of one Locomotive BB22000 or BB26000 and 7 to 14 'Corail' coaches, depending on the service. The geometrical characteristics and axle loads of locomotive and coaches of the test Intercity train are presented in Fig. 2. The

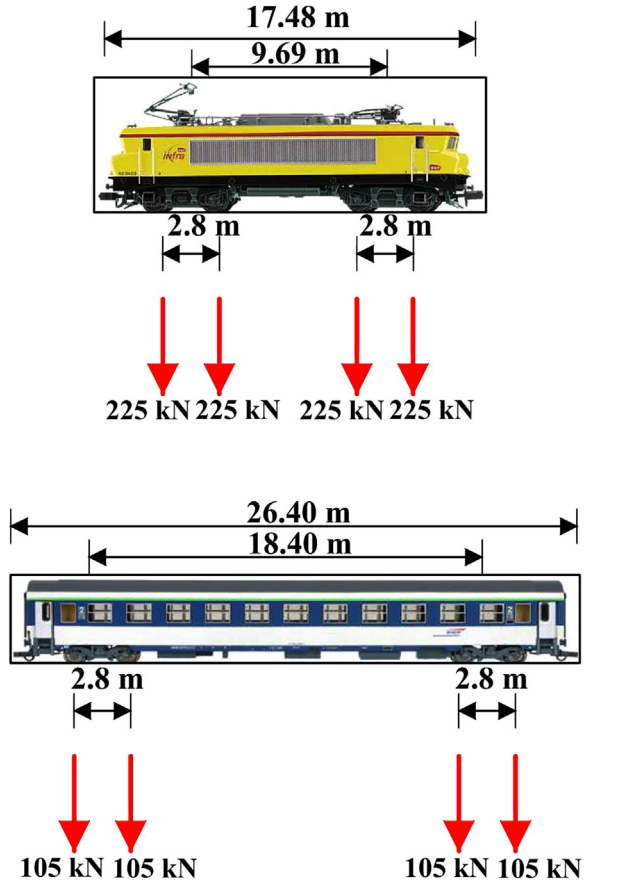

Fig. 2. Geometrical characteristics and axle loads of a locomotive BB22000 and a 'Corail' coach.

locomotive length is 17.48 *m* with an inter-bogie distance of 9.69 *m* and an inter-axles distance of 2.8 *m*. The total mass of the locomotive is 900 *kN*, about 225 kN/axle. Each coach is 26.4 m long. The distance of a pair of bogies for one coach is 18.4 *m* and the distance between bogies of adjacent coaches is 8 m. As for locomotives, the inter-axle distance in 'Corail' coaches is 2.8 m. The total mass of one entire coach is 42 *Mg* and the average load per axle is 105 *kN*. An example of axle-load measurement registered for an Intercity train using the strain gauges glued to the rail (calibrated using a known-load train) is shown in Fig. 3.

The sensors installed in the track-bed were connected to a data logger (HBM-cx22). Once a train running over the platform was detected (from strain gauge signals, used as triggers) a file in MATLAB format was created, recording all the responses of sensors for 45 *s*. The used sampling frequency was 1200 *Hz*. Between April 2014 and August 2014, a total of 8135 trains ran on the experimental site (on both tracks 1 and 2). Using the strain gauge signal it was possible to determine the train typology depending on the axle loading geometrical characteristics and the loading level of each train axle (linearly proportional to the rail measured strain). It appears that a total of 1790 passages of Intercity train were recorded in the period from April 2014 to August 2014 on Track 1. Table 2 presents the number of analysed passages per range of running speeds.

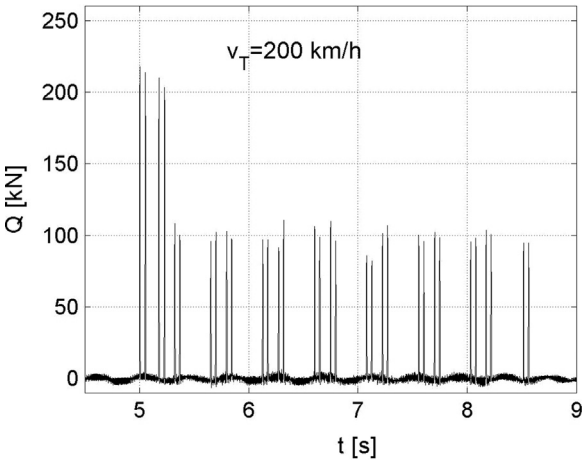

Fig. 3. Strain gauges signal under an Intercity train passage at 200 km/h. The Intercity train of the figure contains on locomotive at the left(4axles) and seven coaches after the locomotive (28 axles).

Table 2
Number of Intercity trains running on track 1 of 'Vierzon Experimental site' between April 2014 and August 2014.

Intercity trains on Track 1	
< 120 km/h	43
120–140 km/h	98
140–160 km/h	604
160–180 km/h	354
> 180 km/h	691
TOTAL	1790

It appears that more than 40% of the passages were at a speed close to 160 km/h (28%) and 200 km/h (14%).

4. Results and discussion

4.1. Signal translation

As the sensors were not installed in the same borehole, the first operation made over the measurements was to translate their signals to simulate the case where all sensors were installed in the same vertical borehole. For this purpose, the sensors signals were moved horizontally to a reference point indicated in Fig. 1b. As the installation horizontal distance between sensors was known (Fig. 1b), accurately translating the signals involved calculating the train speed based on the sensor signals. The train speed was calculated using one signal, determining the positions of peaks from the first two locomotive axles and determining the number of signal positions between these peaks. With a sampling frequency of 1200 *Hz* and a distance of 2.8 m between the two axles, the train speed can be calculated using Eq. (1):

$$v_T = \frac{d_{axles} \cdot fs}{pos_{axles}} \quad (1)$$

where v_T is the train speed, d_{axles} is the distance between the two considered axle peaks (2.8 *m*), f_s is the sampling frequency

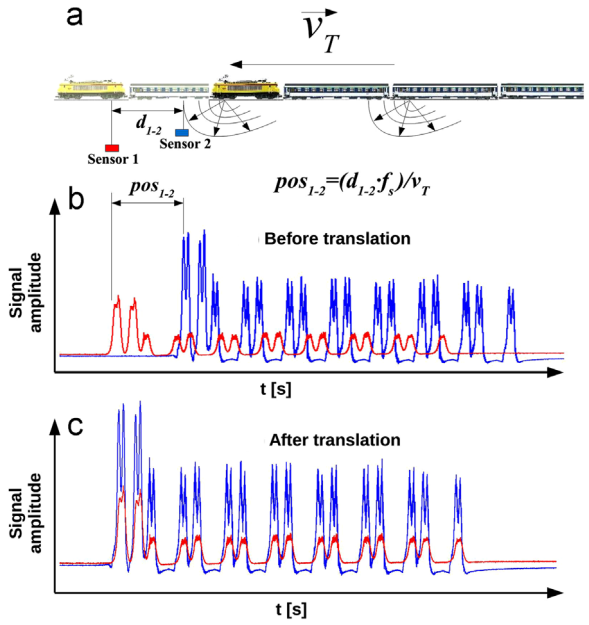

Fig. 4. Scheme of signal translation.

(1200 *Hz*) and pos_{axles} is the number of signal positions between the two considered axle peaks. With the selected sampling frequency and the used method to determine the axle peaks, the accuracy of the train speed determination is $\Delta v = \pm 0.01$ km/h.

Then, a signal translation is performed in order to simulate the case where all the sensors were installed in the same boreholes. Therefore, the horizontal distances between the sensors are known (Fig. 4). The main hypothesis for this operation is that when the peak-axle is recorded in a sensor signal, the train axle is supposed to be just over the sensor in that moment. As the primary (compressive) wave velocity (about $v_p = 1000$ *m/s* for ITL soil) is much faster than the shear wave velocity, the time for a load (axle) to be transmitted from the surface to a sensor can be calculated using Eq. (2):

$$t = \frac{d_{installation}}{v_p} \quad (2)$$

with $d_{installation}$ the installation depth of the sensor, v_p the average primary wave velocity of the considered track profile and t the time for the loading to arrive to the sensor. For instance, when the installation depth is 2 m and an average v_p is 1000 *m/s*, the time for the load to arrive at the sensor is 0.002 *s*. As the sampling frequency gives a sampling period of $\Delta t = \pm 0.0008$ *s*, that time represents about 2 signal positions (even shorter if the sensor is installed closer to the load source). This suggests an insignificant influence on the results obtained under the hypothesis of vertically installed sensors after the translation operation. Consequently, for a train running at the maximum speed on the site (200 km/h), 2 signal positions at the chosen sampling frequency represent an error of 90 *mm*, smaller than the borehole diameter (ø = 110 *mm*). Obviously, this error can be much smaller if the two sensors considered in the calculation are vertically closer. For instance, when the

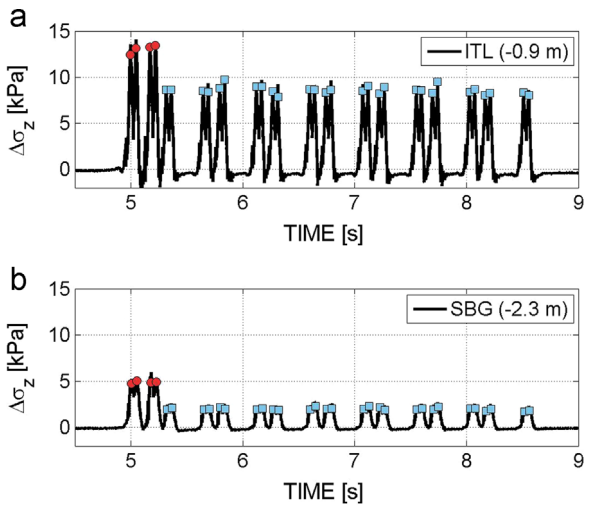

Fig. 5. Raw vertical stress signals for (a) ITL and (b) SBG. Peaks caused by Locomotive and Coaches' axles in $\Delta\sigma_z$ signal are spotted. Train in figure runs at 200 km/h.

vertical strains were calculated based on the displacements estimated from two neighbouring accelerometers.

4.2. Stress response

The stress sensor responses for the 1790 Intercity train passages were first analysed. The raw vertical stress signal at 200 km/h is presented in Fig. 5 for ITL (Fig. 5a, $z=-0.90\ m$) and SBG (Fig. 5b, $z=-2.30\ m$). The locomotive stress peaks (4 peaks) are indicated in the left part of the signals with circles, while the coach stress peaks for each axle are indicated in the right part of the signals with squares. The stress amplitudes $\Delta\sigma_z$ induced by the locomotive axles in ITL are about 14 kPa, while the coach axles induced a $\Delta\sigma_z$ of 8 kPa. Deeper in the track-bed, the axles induced lower stresses in SBG: 5 kPa for the locomotive and 2 kPa for the coaches. Note that the stress amplitude is considered as the difference between the mean stress ($\Delta\sigma_{z=}0$ kPa) and the stress value at each peak.

The stress amplitudes are further analysed separately for each depth (ITL and SBG) and each axle load (locomotive and coach). For each train passage, one stress amplitude value is calculated for locomotives and another for coaches. The locomotive and coach values are the average of each type of peaks (four peaks for locomotives and four times the number of coaches). The evolution of $\Delta\sigma_z$ with speed for both axle types is presented in Fig. 6a for ITL and Fig. 6b for SBG. It appears that the amplification of stress amplitude with train speed is more evident for shallower positions as ITL than for deeper levels as SBG. A quasi-linear amplification is observed in the considered range of speeds. This quasi-linear trend is better defined for SBG where smaller data scatter is obtained. The value of the linear fitting for $v_{T=}0$ km/h corresponds to the $\Delta\sigma_z$ caused by a static axle (11.5 kPa for Locomotive and 5.5 kPa for Coach in the ITL and 4.5 for Locomotive and 1.32 kPa for Coach in the SBG). The stress

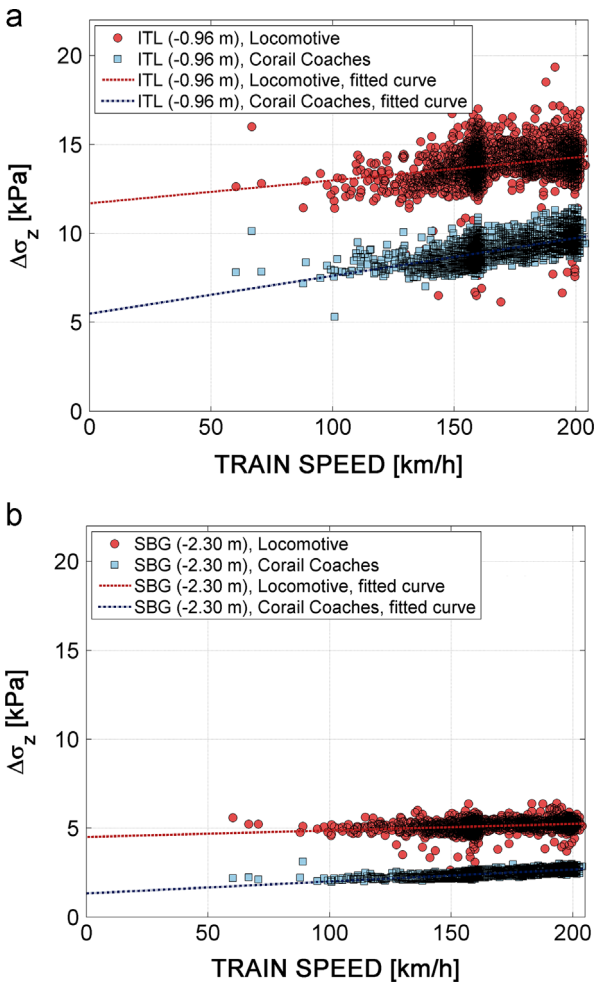

Fig. 6. Vertical stress amplitude caused by Locomotives and Corail Coaches' axles at (a) ITL and (b) SBG.

amplitude ($\Delta\sigma_z$) increase with speed is the same for both axle loads from the origin ($v_{T=}0$ km/h). A 10% amplification in $\Delta\sigma_z$ is identified for locomotive axles in both ITL and SBG. However, the absolute values of the stress amplitudes are quite different for different depths, $\Delta\sigma_z$ rapidly attenuating with depth. Larger data scatter is found in ITL, which is closer to the load source. The values for locomotives are also largely scattered due to the smaller number of locomotive peaks per train (compared to coach peaks) which can be used to calculate the average value. A second reason for this higher dispersion compared to lower axle loads (Coaches' axles) could be the force irregularities in the wheel/rail contact induced by the axle of the locomotive (the heaviest axles in the train). These amplifications of axle loadings appeared also due to the wheel roundness defects. These defects may impact the wheel/rail contact. Consequently, higher loadings and responses appeared for some of the recorded train's passages in the low-frequency range (where most of the energy inducing deflections developed). The $\Delta\sigma_z$ variations in ITL (where more dispersion appears in Fig. 6a and Fig. 6b) for locomotive and coach around their average values are presented in Tables 3 and 4, respectively. No impact was

Table 3
Normal distribution parameters (mean value μ, standard deviation σ and variation coefficient CV) for stress amplitudes ($\Delta\sigma_z$) caused by Locomotives axles measured in the Interlayer from 'Vierzon experimental site'.

		Speed influence/interlayer (−0.9 m) locomotive (22.5 mg/axle)				
		< 120 km/h	120–140 km/h	140–160 km/h	160–180 km/h	> 180 km/h
$\Delta\sigma_z$	μ (kPa)	13	13.1	13.7	14.1	14.2
	σ (kPa)	0.903	1.03	1.15	1.05	1.18
	CV (%)	**6.97**	**7.92**	**8.36**	**7.45**	**8.35**

Table 4
Normal distribution parameters (mean value μ, standard deviation σ and variation coefficient CV) for stress amplitudes ($\Delta\sigma_z$) caused by Corail Coaches axles measured in the Interlayer from 'Vierzon experimental site'.

		Speed influence/interlayer (−0.9 m) corail coaches (10.5 mg/axle)				
		< 120 km/h	120–140 km/h	140–160 km/h	160–180 km/h	> 180 km/h
$\Delta\sigma_z$	μ (kPa)	8.21	8.29	8.71	9.07	9.65
	σ (kPa)	0.755	0.496	0.608	0.57	0.594
	CV (%)	**9.2**	**5.98**	**6.98**	**6.29**	**6.16**

observed on the variation coefficient due to increasing speed: it remained around the average value for each speed range and for each type of axle load. As expected, no high variability of registered data was found for higher speeds due to the dynamic effects of train loading. The registered data for higher speeds are assumed to follow the same distribution around their average values.

4.3. Accelerometer response

Fig. 7 shows the filtered ($f_c = 25\ Hz$) accelerometer signals at $v_T = 200$ km/h, and at different depths (ITL–Fig. 7a, TL–Fig. 7b, SBG–Fig. 7c). The signals are filtered to obtain the accelerometer amplitudes (Δa_z) which cause more than 98% of deflections (Lamas-Lopez et al. 2014). A low-pass Butterworth filter with a cut-off frequency of $f_c = 25\ Hz$ was used for this purpose. The acceleration at axle peaks are identified and are indicated in Fig. 7. The circles correspond to the locomotives axles and the squares correspond to coaches. The acceleration amplitudes Δa_z are measured from the positive part of each axle peak to the average acceleration of the signal ($\Delta a_z = 0\ m/s^2$). The value of Δa_z is highly attenuated from ITL to TL, 300 mm deeper. The amplitudes for the locomotive are double those for coaches. As for $\Delta\sigma_z$, two values are calculated for each train passage: an average Δa_z for the 4 locomotive axles and another average Δa_z for coach axles. The evolution of Δa_z with a train speed for the 1790 passages is presented in Fig. 8, for ITL (Fig. 8a), TL (Fig. 8b) and SBG (Fig. 8c). From the acceleration amplitudes at each track-bed level, it can be appreciated that most of the amplitudes causing deflections attenuated in the stiffer ITL layer. The acceleration amplitudes increase with train speed following a parabolic relation depending on the square value of the train speed for the range of tested speeds. This parabolic relationship is related to the fact that the kinematic energy transmitted to the system increases with the axle's mass and the train speed is proportional to the acceleration amplitude.

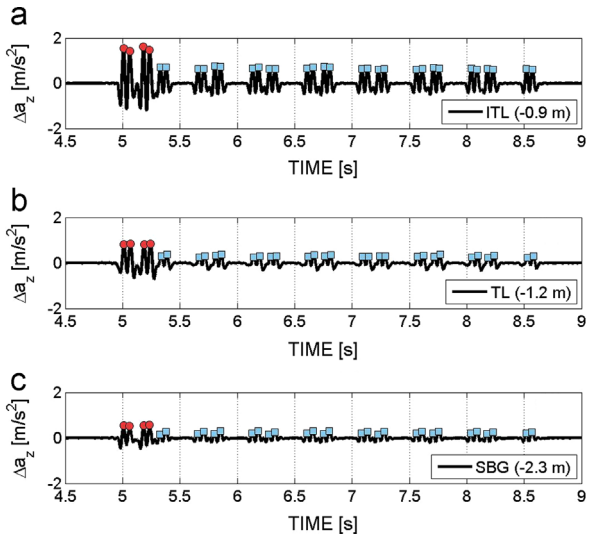

Fig. 7. Vertical acceleration signals ($f_c = 25$ Hz) for (a) ITL, (b) TL and (c) SBG. Peaks caused by Locomotive and Coaches' axles in Δaz signal are spotted. Train in figures runs at 200 km/h.

4.4. Particle velocity response

A Butterworth high-pass filter ($f_c = 1.5\ Hz$) was applied to avoid the baseline effects during the integration operation. This high-pass filter was applied to avoid the very low-frequencies signal that are not possible to be well registered by this kind of sensors (Boore, 2001). Lower cut-off frequencies induce baseline defects for this accelerometer model. After a first integration of Δa_z, the particle velocity signal Δv_z was obtained. As for the stress and acceleration, the amplitudes of particle velocity were calculated as the difference between the maximum value at axle positions and the average of the particle velocity. The amplitude average was calculated for each train passage, with the kind of axles taken into account (locomotive and coaches). Fig. 9 presents the evolution of Δv_z with train speed for the 1790 passages at three different depths (ITL at $-0.90\ m$, TL at $-1.20\ m$ and SBG at $-2.3\ m$). A quasi-linear trend can be identified for all depths and for both axle loads.

4.5. Displacement magnitudes

Another high-pass Butterworth filter ($f_c = 1.5\ Hz$) was applied to the particle velocity signals prior to a second integration to obtain the displacement amplitude signal Δd_z.

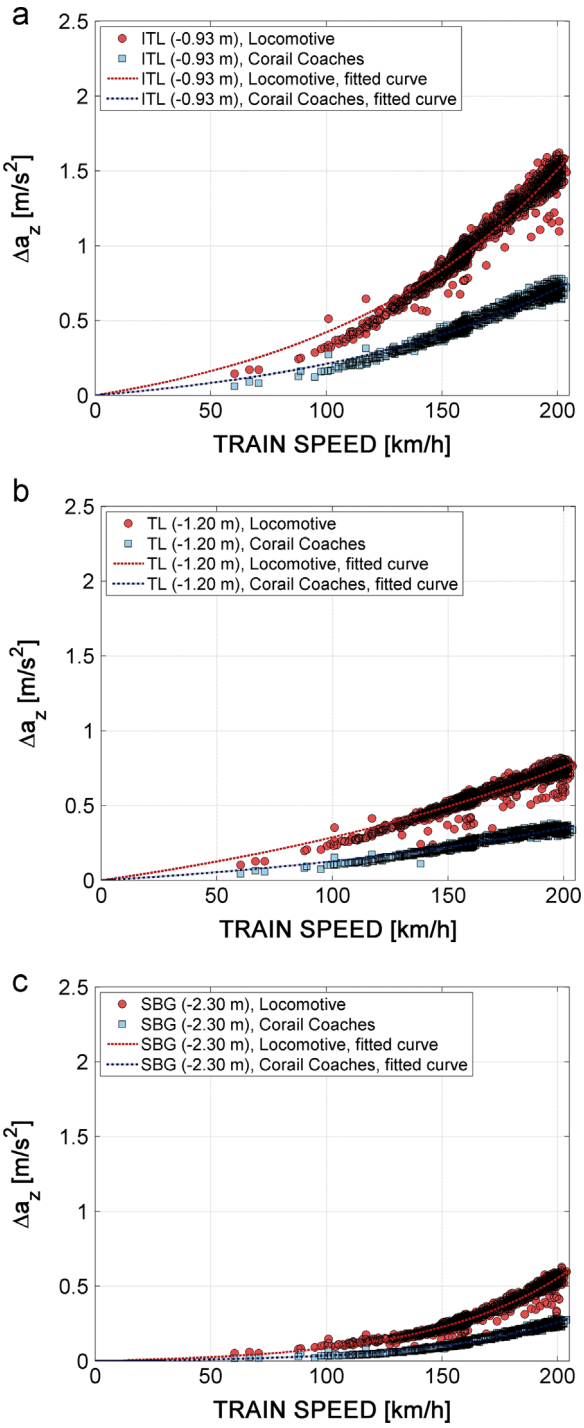

Fig. 8. Vertical acceleration amplitude ($f_c = 25$ Hz) caused by Locomotives and Corail Coaches' axles at (a) ITL, (b) TL and (c) SBG.

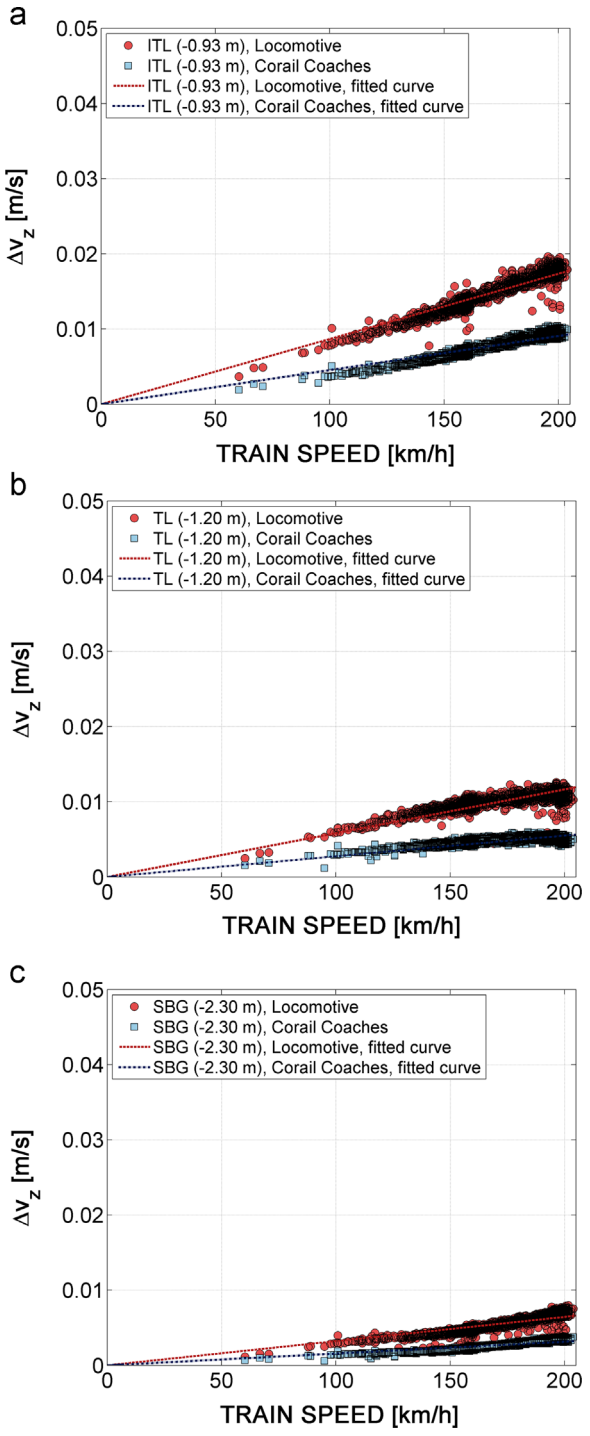

Fig. 9. Vertical velocity amplitude caused by Locomotives and Corail Coaches' axles at (a) ITL, (b) TL and (c) SBG.

Because of the border conditions imposed to the integration process at the beginning and at the end of the integrated signal ($\Delta d_z(t_0)=0$; $\Delta d_z(t_n)=0$), both negative (downward) and positive (upward) deflections were obtained (Fig. 10a). However, from the direct measurements on surface (using LVDTs on a sleeper), only downward deflections are registered if the sleepers work correctly. In the previous studies, several authors (Le Pen et al., 2014; Priest and Powrie, 2009; Yang et al., 2009) reported the same displacement response with positive and negative values, obtained by integrating the signals of geophones or accelerometer. The total displacement signal should be considered as if the displacements occurred in a downward direction only. Thereby, the displacement amplitudes caused by every train axle in the Δd_z signal were calculated as the sum of the negative part and the positive maximum point adjacent to the axle as presented in Fig. 10a

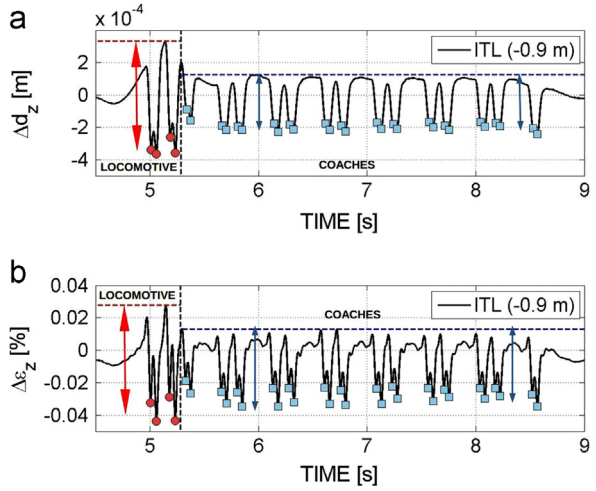

Fig. 10. Peak definition using the (a) vertical displacement signal at ITL and (b) estimated vertical strain between two accelerometers installed in the ITL. Train in figure runs at 200 km/h.

(Le Pen et al., 2014). An example of the estimated vertical deformation amplitudes ($\Delta\varepsilon_z$) using displacements at different depths is shown in Fig. 10b. The amplitudes in this figure are calculated in the same manner the displacement amplitudes were calculated.

The average Δd_z amplitudes were calculated for the locomotives and axles at every monitored depth using this method. The results obtained for the 1790 passages are presented in Fig. 11. The displacement amplitudes Δd_z also follow a linear trend depending on two parameters: the deflection at static load and the deflection amplification with speed. These two parameters depend mainly on the axle load, the depth and the train speed.

It is observed that the displacement amplitudes increase even at the low speeds (there is not a cutting-off speed as supposed by Madshus and Kaynia 2000). Higher deflection amplifications with train speed are found in shallower layers. The amplification of different loads (locomotive and coaches) at the same depth follows the same trend. The Δd_z amplitudes largely attenuated through ITL.

However, the calculated displacement for speeds lower than 75 km/h appears abnormally low. This is because for these speeds some very low frequencies as that excited by the half-length coach were erased when applying the high-pass Butterworth filter. For instance, at 60 km/h, the half-length coach excited frequency is 1.8 Hz (one of the most energetic wavelengths) and it is partly filtered by the Butterworth high-pass filter. As for the stress, the variations around the average value of Δd_z by range of train speed are determined for ITL (where more data scatter appears in Fig. 11) and presented in Table 5 (locomotive) and Table 6 (coaches). It is observed that there is no influence of data scatter around the average values: the standard deviation remains stable around the average values for each speed range. The displacement amplification with train speed was consistent and stable over time. The amplifications for higher speeds could be inferred from these results following the same trend of material response.

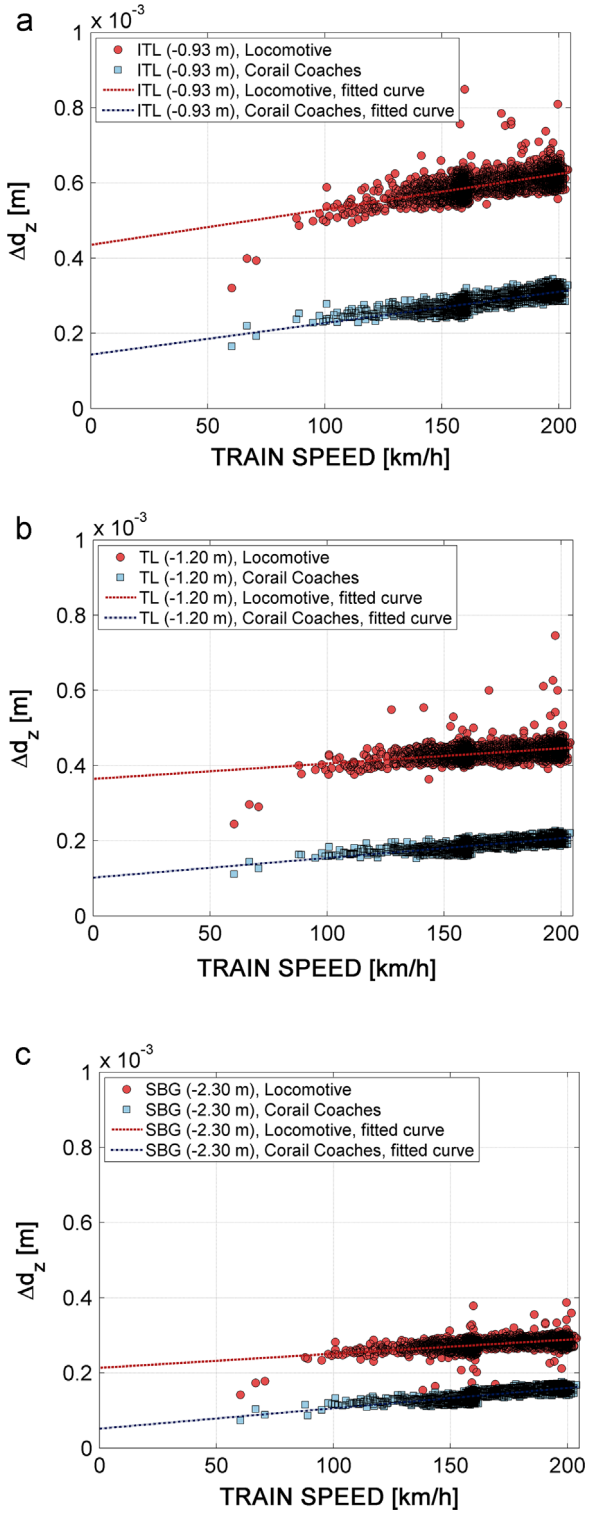

Fig. 11. Vertical displacement amplitude caused by Locomotives and Corail Coaches' axles at (a) ITL, (b) TL and (c) SBG.

As the sensor signals are considered as being in the same vertical position, from the deflections at different levels, the

Table 5
Normal distribution parameters (mean value μ, standard deviation σ and variation coefficient CV) for displacement amplitudes (Δd_z) caused by Locomotives axles measured in the Interlayer from 'Vierzon experimental site'.

		Speed influence/interlayer (−0.9 m) locomotive (22.5 mg/axle)				
		< 120 km/h	120–140 km/h	140–160 km/h	160–180 km/h	> 180 km/h
Δd_z	μ (mm)	$5.18 \cdot 10^{-4}$	$5.64 \cdot 10^{-4}$	$5.83 \cdot 10^{-4}$	$5.95 \cdot 10^{-4}$	$6.17 \cdot 10^{-4}$
	σ (mm)	$5.02 \cdot 10^{-5}$	$2.3 \cdot 10^{-5}$	$3.11 \cdot 10^{-5}$	$2.94 \cdot 10^{-5}$	$2.48 \cdot 10^{-5}$
	CV (%)	**9.71**	**4.08**	**5.34**	**4.94**	**4.02**

Table 6
Normal distribution parameters (mean value μ, standard deviation σ and variation coefficient CV) for displacement amplitudes (Δd_z) caused by Corail Coaches axles measured in the Interlayer from 'Vierzon experimental site'.

		Speed influence/interlayer (−0.9 m) corail coaches (10.5 mg/axle)				
		< 120 km/h	120–140 km/h	140–160 km/h	160–180 km/h	> 180 km/h
Δd_z	μ (mm)	$2.44 \cdot 10^{-4}$	$2.59 \cdot 10^{-4}$	$2.7 \cdot 10^{-4}$	$2.84 \cdot 10^{-4}$	$3.07 \cdot 10^{-4}$
	σ (mm)	$2.04 \cdot 10^{-5}$	$1.12 \cdot 10^{-5}$	$1.39 \cdot 10^{-5}$	$1.54 \cdot 10^{-5}$	$1.37 \cdot 10^{-5}$
	CV (%)	**8.36**	**4.32**	**5.14**	**5.43**	**4.17**

vertical strains can be estimated using Eq. (3):

$$\Delta\varepsilon_z = (\Delta d_2 - \Delta d_1) \cdot 100/d_{vert} \quad (3)$$

where Δd_2 is the displacement signal at the shallower accelerometer, Δd_1 is the displacement signal at the deeper accelerometer and d_{vert} is the vertical distance between both sensors. The vertical distance between the accelerometers in ITL and TL is 0.3 m, and 1.10 m between the sensors in TL and SBG.

The estimated vertical strain amplitudes $\Delta\varepsilon_z$ for the 1790 passages are presented in Fig. 12 for ITL (Fig. 12a) and SBG (Fig. 12b). Its variation with speed also follows a quasi-linear trend. For each given depth (ITL or SBG), both axle loads (locomotive and coach) caused the same strain amplitude increase with the growth of train speed (in absolute values from the origin $v_{T=}0$ km/h).

More dispersion of locomotive values appear in ITL but further analysis shows that the points'escaping' upwards from the linear fitting line (till $\Delta\varepsilon_{z=}0.2\%$) are also due to the 'attacking axles' (first axle of a train, that commonly loads the track at a higher level compared to similar axle loads) that sometimes induces higher load levels if there are irregularities in wheel/rail contact related to wheel roundness defects. The heavier the axle, the greater the impact of wheel roundness defects on the loading amplification. Though the first locomotive axle sometimes caused an increase of deflections in the shallower layers, it attenuated mostly when the loading passed through ITL compared to SBG. This dynamic excitation affects more the shallower layers. Thus, the difference between the deflections at different depths could be higher in some of the considered passages for these first axles.

The variation of $\Delta\varepsilon_z$ around the mean value (for the 5 considered speed ranges) is presented in Tables 7 and 8.

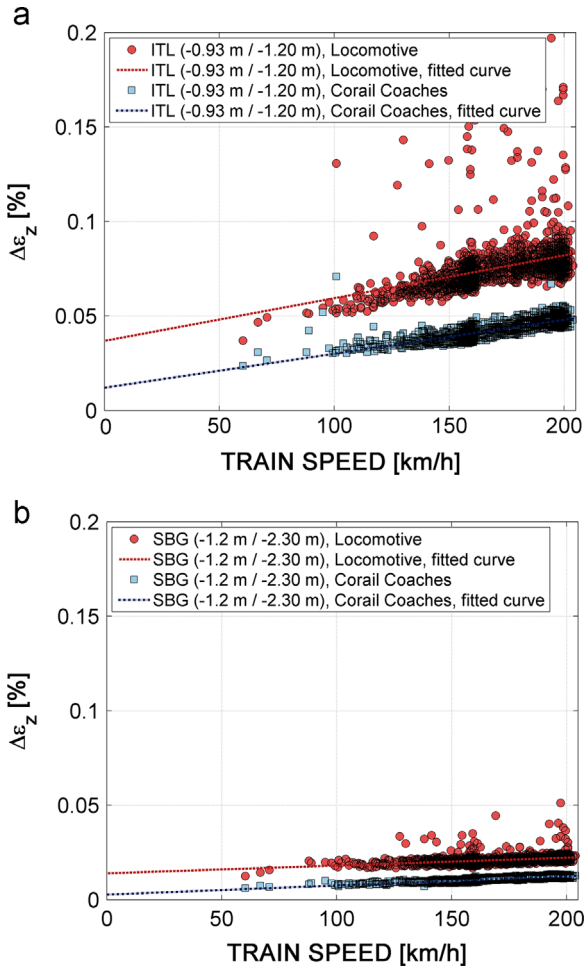

Fig. 12. Vertical strain amplitude caused by Locomotives and Corail Coaches' axles at (a) ITL and (b) SBG.

Table 7
Normal distribution parameters (mean value μ, standard deviation σ and variation coefficient CV) for vertical strain amplitudes ($\Delta\varepsilon_z$) caused by Locomotives axles measured in the Interlayer from 'Vierzon experimental site'.

		Speed influence/interlayer (−0.9 m) locomotive (22.5 mg/axle)				
		< 120 km/h	120–140 km/h	140–160 km/h	160–180 km/h	> 180 km/h
$\Delta\varepsilon_z$	μ (%)	0.0589	0.0659	0.072	0.0758	0.0803
	σ (%)	0.0143	0.0112	0.0131	0.0108	0.0120
	CV (%)	**24.3**	**17.1**	**18.2**	**14.2**	**15**

Table 8
Normal distribution parameters (mean value μ, standard deviation σ and variation coefficient CV) for vertical strain amplitudes ($\Delta\varepsilon_z$) caused by Corail Coaches axles measured in the Interlayer from 'Vierzon experimental site'.

		Speed influence/interlayer (−0.9 m) corail coaches (10.5 mg/axle)				
		< 120 km/h	120–140 km/h	140–160 km/h	160–180 km/h	> 180 km/h
$\Delta\varepsilon_z$	μ (%)	0.035	0.0362	0.0393	0.0419	0.0474
	σ (%)	0.00753	0.0024	0.00247	0.00289	0.00278
	CV (%)	**21.5**	**6.64**	**6.28**	**6.89**	**5.87**

The results show that there is no effect of speed on the variation coefficient (CV) around the mean value: the standard deviation remains stable at different speeds for locomotive and decreases for lower loads–the coach load. As no train speed effect was considered for the registered trains and a low dispersion of data was found, the evolution of vertical strain amplitudes with different train loads can be inferred from these results following the average value evolution for a given train speed.

4.6. Resilient modulus

As the vertical stress $\Delta\sigma_z$ and vertical strain $\Delta\varepsilon_z$ amplitudes were calculated for each train passage, it is possible to estimate the resilient modulus M_r of each track-bed material (ITL and SBG) using Eq. (4):

$$M_R = \frac{\Delta\sigma_z}{\Delta\varepsilon_z} \tag{4}$$

This modulus represents the slope of the line that links the origin to the maximum stress in the hysteresis loops. The results for the locomotive and coaches are presented in Fig. 13. Note that this M_r calculated from the measured vertical stress and the estimated strain amplitudes includes the inertia effect (mass impact) of the entire structure and loading system (train axles). Therefore, the calculated M_r values in this study are different from the values that can be obtained in the laboratory (through cyclic triaxial tests for instance). A higher impact of train speed on M_r is identified in ITL compared to SBG where M_r is more stable: an average decrease of about 25% is found

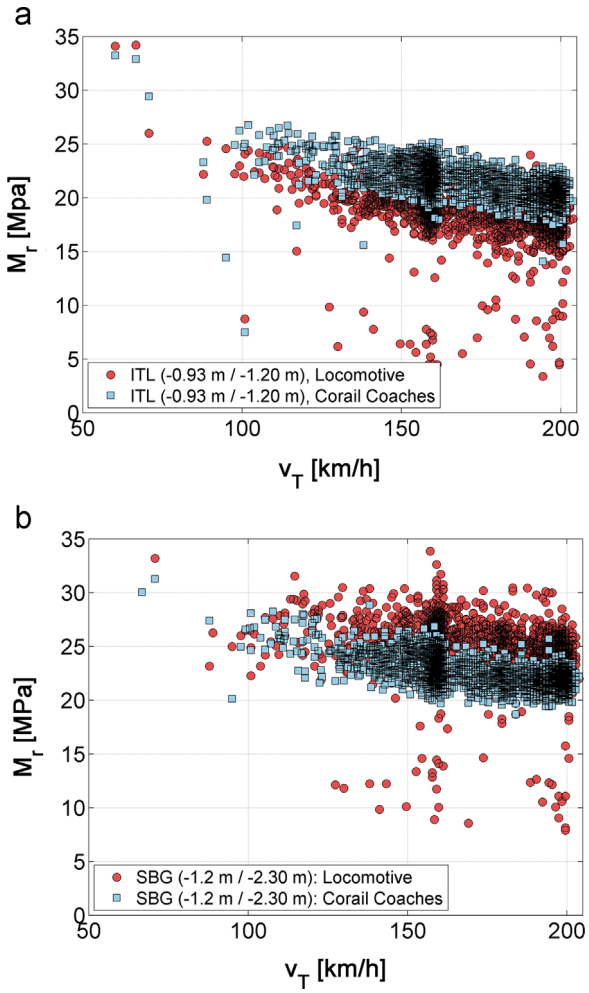

Fig. 13. Estimated resilient modulus for Locomotives and Corail Coaches loadings at (a) ITL and (b) SBG.

for M_r in ITL, while a 10% decrease is estimated in SBG. The obtained ratio between $\Delta\sigma_z$ and $\Delta\varepsilon_z$ is the same for both axle loads. This means that the calculation method adopted is valid for both loadings, and this also shows the reliability of stress measurements under different axle loads. The scattered M_r values below the general trend are caused by the higher response of the track-bed material due to the 'attacking axle' (first locomotive axle) loading amplification effect on the measurements.

5. Conclusion

The mechanical behaviour of a French conventional track-bed was investigated through field monitoring. Emphasis was put on the effect of train speed. The evolution and dispersion of data was presented and analysed.

The Intercity train was selected to be analysed given that more than 40% of trains running on the experimental site involved this type. A total of 1790 trains were registered from April to August 2014. The analysis of the recorded data showed that the amplitudes of vertical stress and strain caused by train axles increased with the increase of speed. The speed

effect on the stress and strain amplitudes attenuated over depth. The axles of locomotive caused a stress of 12-14 kPa in ITL, while the stress amplitude was about 5 kPa in SBG for locomotives and coaches. The amplification ratio of $\Delta\sigma_z$ applied by the axle of locomotive is approximately 10% in ITL and SBG, while this amplification ratio increases up to 20-30% for lower loads (coaches) in the case of 200 km/h speed. The amplification of stress and strain with speed growth in absolute value is the same for both ITL and SBG. The vertical strains $\Delta\varepsilon_z$ by locomotive are in the range from 0.03% to 0.07% in ITL, and from 0.015% to 0.02% in SBG. The amplification of $\Delta\varepsilon_z$ at 200 km/h can double the lowest strain obtained in the case of lower speeds. The resilient modulus M_r estimated from the ratios of $\Delta\sigma_z$ to $\Delta\varepsilon_z$ showed a decreasing trend with the growth of speed and the maximum reduction was 25% for shallower layers, like the ITL. The decrease of the resilient modulus with increasing speed was found smaller for deeper layers, like the SBG. The similarity of the modulus values for both axle loads is evidence of an insignificant effect of the loading level.

Acknowledgments

This paper reports part of the 'INVICSA' research project funded by SNCF-RESEAU and the ANRT with a CIFRE funding number 2012/1150. The authors are grateful to Jean-Michel Pissot, Christophe Gouel and Victor Tuong for providing their technical advice and performing the monitoring work. The authors would also like to thank the track maintenance SNCF brigade at Vierzon, especially their planning coordinator Ludovic Gaveau, without whom this monitoring work would not have been accomplished.

References

Alves Costa, P., Calçada, R., Silva Cardoso, A., Bodare, A., 2010. Influence of soil non-linearity on the dynamic response of high-speed railway tracks. Soil Dyn. Earthq. Eng 30, 221–235. http://dx.doi.org/10.1016/j.soildyn.2009.11.002.

Alves Fernandes, V., 2014. Numerical Analysis of Nonlinear Soil Behavior and Heterogeneity Effects on Railway Track Response. Ecole Centrale Paris.

Aw, E.S., 2007. Low Cost Monitoring System to Diagnose Problematic Rail Bed : Case Study at a Mud Pumping Site. Massachusetts Institute of Technology.

Bian, X., Jiang, H., Cheng, C., Chen, Y., Chen, R., Jiang, J., 2014. Full-scale model testing on a ballastless high-speed railway under simulated train moving loads. Soil Dyn. Earthq. Eng 66, 368–384. http://dx.doi.org/10.1016/j.soildyn.2014.08.003.

Boore, D.M., 2001. Effect of Baseline Corrections on Displacements and Response Spectra for Several Recordings of the 1999 Chi-Chi, Taiwan, Earthquake. Bull. Seismol. Soc. Am. 91, 1199–1211.

Bowness, D., Lock, a C., Powrie, W., Priest, J. a, Richards, D.J., 2007. Monitoring the dynamic displacements of railway track. Proc. Inst. Mech. Eng. Part F J. Rail Rapid Transit 221, 13–23. http://dx.doi.org/10.1243/0954409JRRT51.

Chen, R., Zhao, X., Wang, Z., Jiang, H., Bian, X., 2013. Experimental study on dynamic load magnification factor for ballastless track-subgrade of high-speed railway. J. Rock Mech. Geotech. Eng 5, 306–311. http://dx.doi.org/10.1016/j.jrmge.2013.04.004.

Connolly, D., Giannopoulos, a, Forde, M.C., 2013. Numerical modelling of ground borne vibrations from high speed rail lines on embankments. Soil Dyn. Earthq. Eng 46, 13–19. http://dx.doi.org/10.1016/j.soildyn.2012.12.003.

Connolly, D.P., Kouroussis, G., Giannopoulos, a, Verlinden, O., Woodward, P.K., Forde, M.C., 2014. Assessment of railway vibrations using an efficient scoping model. Soil Dyn. Earthq. Eng 58, 37–47. http://dx.doi.org/10.1016/j.soildyn.2013.12.003.

Costa, P.A., Colaço, A., Calçada, R., Cardoso, A.S., 2015. Critical speed of railway tracks. Detailed and simplified approaches. Transp. Geotech 2, 30–46. http://dx.doi.org/10.1016/j.trgeo.2014.09.003.

Cui, Y., Duong, T.V., Tang, A.M., Dupla, J.-C., Calon, N., Robinet, A., 2013. Investigation of the hydro-mechanical behaviour of fouled ballast. J. Zhejiang Univ. Sci. A 14, 244–255. http://dx.doi.org/10.1631/jzus.A1200337.

Cui, Y.-J., Lamas-Lopez, F., Trinh, V.N., Calon, N., D'Aguiar, S.C., Dupla, J.-C., Tang, A.M., Canou, J., Robinet, A., 2014. Investigation of interlayer soil behaviour by field monitoring. Transp. Geotech 1, 91–105. http://dx.doi.org/10.1016/j.trgeo.2014.04.002.

Duong, T.V., Cui, Y.J., Tang, a M., Calon, N., Robinet, A., 2014b. Assessment of conventional French railway sub-structure: a case study. Bull. Eng. Geol. Environ., 1–12. http://dx.doi.org/10.1007/s10064-014-0575-y.

Duong, T.V., Cui, Y.-J., Tang, A.M., Dupla, J.-C., Canou, J., Calon, N., Robinet, A., 2014a. Investigating the mud pumping and interlayer creation phenomena in railway sub-structure. Eng. Geol. 171, 45–58. http://dx.doi.org/10.1016/j.enggeo.2013.12.016.

Duong, T.-V., Tang, A.-M., Cui, Y., Trinh, V.-N., Dupla, J.-C., Calon, N., Canou, J., Robinet, A., 2013. Effects of fines and water contents on the mechanical behavior of interlayer soil in ancient railway sub-structure. Soils Found. 53, 868–878.

Fröhling, R.D., 1997. Deterioration of railway track due to dynamic vehicle loading and spatially varying track stiffness. University of Pretoria.

Gunn, D. a, Jackson, P.D., Entwisle, D.C., Armstrong, R.W., Culshaw, M.G., 2003. Predicting subgrade shear modulus from existing ground models. NDT E Int 36, 135–144. http://dx.doi.org/10.1016/S0963-8695(02)00052-X.

Hall, L., 2003. Simulations and analyses of train-induced ground vibrations in finite element models. Soil Dyn. Earthq. Eng 23, 403–413. http://dx.doi.org/10.1016/S0267-7261(02)00209-9.

Hall, L., Bodare, a, 2000. Analyses of the cross-hole method for determining shear wave velocities and damping ratios. Soil Dyn. Earthq. Eng. 20, 167–175. http://dx.doi.org/10.1016/S0267-7261(00)00048-8.

Hendry, M., Barbour, L., Hughes, D. a, 2010. Track displacement and energy loss in a railway embankment. Proc. ICE–Geotech. Eng. 163, 3–12. http://dx.doi.org/10.1680/geng.2010.163.1.3.

Hendry, M.T., 2007. Train-induced Dynamic Response of Railway Track and Embankments on Soft Peaty. University of Saskatchewan.

Hendry, M.T., 2011. The geomechanical behaviour of peat foundations below rail-track structures. University of Saskatchewan.

Hendry, M.T., Martin, C.D., Barbour, S.L., 2013. Measurement of cyclic response of railway embankments. Can. Geotech. J. 50, 1–14.

Kempfert, H.G., Hu, Y., 1999. Measured dynamic loading of railway underground, in: Proceedings of the XI Panamerican Conference on Soil Mechanics and Geotechnicall Engineering. Foz do Iguazu, Brazil, p. 5.

Kim, D.-S., Shin, M.-K., Park, H.-C., 2001. Evaluation of density in layer compaction using SASW method. Soil Dyn. Earthq. Eng 21, 39–46. http://dx.doi.org/10.1016/S0267-7261(00)00076-2.

Kouroussis, G., 2009. Modélisation des effets vibratoires du trafic ferroviaire sur l'environnement. Polytech Mons, Belgium.

Lamas-Lopez, F., Alves Fernandes, V., Cui, Y., Costa D'Aguiar, S., Calon, N., Canou, J., Dupla, J.-C., Tang, A.-M., Robinet, A., 2014a. Assessment of the double integration method using accelerometers data for conventional railway platforms. In: Development and Maintenance. Ajaccio, Corsica, pp. 1–19.

Lamas-Lopez, F., Cui, Y.-J., Calon, N., Costa D'Aguiar, S., 2016. Geotechnical auscultation of a French conventional railway track-bed for maintenance purposes. Soils Found., 56.

Lamas-Lopez, F., Cui, Y., Calon, N., Robinet, A., Dupla, J.-C., Costa D'Aguiar, S., Tang, A.-M., Canou, J., 2014b. Field instrumentation to study the behaviour of a conventional railway platform. In: Marne la Vallée.

Le Pen, L., 2008. Track behaviour: the importance of the sleeper to ballast interface.

Le Pen, L., Watson, G., Powrie, W., Yeo, G., Weston, P., Roberts, C., 2014. The behaviour of railway level crossings: Insights through field monitoring. Transp. Geotech 1, 201–213. http://dx.doi.org/10.1016/j.trgeo.2014.05.002.

Madshus, C., Kaynia, a M., 2000. High-Speed Railway Lines on Soft Ground: Dynamic Behaviour At Critical Train Speed. J. Sound Vib. 231, 689–701. http://dx.doi.org/10.1006/jsvi.1999.2647.

Madshus, C., Lacasse, S., Kaynia, A., Harvik, L., 2004. Geodynamic Challenges in High Speed Railway Projects. Geotech. Eng. Transp. Proj, 192–215. http://dx.doi.org/10.1061/40744(154)6.

Mishra, D., Tutumluer, E., Boler, H., Hyslip, J.P., Sussman, T., 2014. Instrumentation and Performance Monitoring of Railroad Track Transitions using Multidepth Deflectometers and Strain Gauges, in: 93rd Annual Meeting of the Transportation Research Board. Washington, DC.

Powrie, W., Yang, L. a, Clayton, C.R.I., 2007. Stress changes in the ground below ballasted railway track during train passage. Proc. Inst. Mech. Eng. Part F J. Rail Rapid Transit 221, 247–262. http://dx.doi.org/10.1243/0954409JRRT95.

Priest, J. a, Powrie, W., Grabe, P.J., Clayton, C.R.I., Yang, L., 2010. Measurements of transient ground movements below a ballasted railway line. Géotechnique 60, 667–677. http://dx.doi.org/10.1680/geot.7.00172.

Priest, J.A., Powrie, W., 2009. Determination of Dynamic Track Modulus from Measurement of Track Velocity during Train Passage. J. Geotech. Geoenvironmental Eng 135, 1732–1740.

Sawangsuriya, A., 2012. Wave Propagation Methods for Determining Stiffness of Geomaterials in. "Wave Processes in Classical and New Solids.", 44.

Sheng, X., Jones, C.J.C., Thompson, D.J., 2004. A theoretical model for ground vibration from trains generated by vertical track irregularities 272, 937–965. http://dx.doi.org/10.1016/S0022-460X(03)00782-X.

Trinh, V.-N., 2011. Comportement hydromécanique des matériaux constitutifs de plateformes ferroviaires anciennes. Université Paris-Est, Marne la Vallée.

Trinh, V.N., Tang, A.M., Cui, Y.-J., Dupla, J.-C., Canou, J., Calon, N., Lambert, L., Robinet, A., Schoen, O., 2012. Mechanical characterisation of the fouled ballast in ancient railway track substructure by large-scale triaxial tests. Soils Found. 52, 511–523. http://dx.doi.org/10.1016/j.sandf.2012.05.009.

Woodward, P.K., Laghrouche, O., Connolly, D., El-Kacimi, A., 2013. Ground dynamics of high-speed trains crossing soft soils. 2013 World Congress on Railway Research.

Xu, X., Jiang, H.G., Bian, X.C., Chen, Y.M., 2013. Accumulative settlement of saturated silt subgrade under cyclic traffic-loading. In: Advances in Environmental Vibration; Sixth International Symposium on Environmental Vibration: Prediction. Monitoring, Mitigation and Evaluation, Shanghai, pp. 493–501.

Yang, L.A., Powrie, W., Priest, J.A., 2009. Dynamic Stress Analysis of a Ballasted Railway Track Bed during Train Passage. J. Geotech. Geoenviron.Eng 135, 680–689. http://dx.doi.org/10.1061/(ASCE)GT.1943-5606.0000032.